ALGORITHMS FOR PROPAGATING UNCERTAINTY ACROSS HETEROGENEOUS DOMAINS

H. CHO[†], X. YANG[‡], D. VENTURI[§], AND G. E. KARNIADAKIS[†¶]

Abstract. We address an important research area in stochastic multi-scale modeling, namely the propagation of uncertainty across heterogeneous domains characterized by partially correlated processes with vastly different correlation lengths. This class of problems arise very often when computing stochastic PDEs and particle models with stochastic/stochastic domain interaction but also with stochastic/deterministic coupling. The domains may be fully embedded, adjacent or partially overlapping. The fundamental open question we address is the construction of *proper* transmission boundary conditions that preserve global statistical properties of the solution across different subdomains. Often, the codes that model different parts of the domains are black-box and hence a domain decomposition technique is required. No rigorous theory or even effective empirical algorithms have yet been developed for this purpose, although interfaces defined in terms of functionals of random fields (e.g., multi-point cumulants) can overcome the computationally prohibitive problem of preserving sample-path continuity across domains. The key idea of the different methods we propose relies on combining local reduced-order representations of random fields with multi-level domain decomposition. Specifically, we propose two new algorithms: The first one enforces the continuity of the conditional mean and variance of the solution across adjacent subdomains by using Schwarz iterations. The second algorithm is based on PDE-constrained multi-objective optimization, and it allows us to set more general interface conditions. The effectiveness of these new algorithms is demonstrated in numerical examples involving elliptic problems with random diffusion coefficients, stochastically advected scalar fields, and nonlinear advection-reaction problems with random reaction rates.

Key words. Multi-scale stochastic modeling, Schwarz methods, parallel domain decomposition, dimensionality reduction.

AMS subject classifications. 60H35, 34F05.

1. Introduction.

Propagating uncertainty across different domains is a problem of major interest in many areas of mathematics and physics, e.g., in modeling random heterogeneous materials [37,39], coarse-graining atomistic and mesoscopic systems [18,19,25,43,54], coupling atomistic to continuum models [24,30,31] or stochastic simulations involving partial differential equations (PDEs) relying on distinct randomness on different subdomains [21–23, 45, 50].

This class of problems can be addressed by using *stochastic domain decomposition methods* [15, 26, 34, 49, 51]. One of the most critical aspects of these methods is the construction of proper transmission boundary conditions to propagate the stochastic solution across different subdomains. A straightforward extension of classical deterministic algorithms [20, 35], e.g., based on Monte Carlo or sparse grid probabilistic collocation [6, 7] yields prohibitively expensive schemes, since the interface operator has to be applied to each solution sample. On the other hand, interfaces defined in terms of *functionals* of the stochastic solution (e.g., multi-point cumulants) can yield, in principle, a tremendous reduction in computational cost. However, very few rigorous theories or even empirical algorithms have been developed to perform domain decomposition in stochastic simulations with functional interfaces [3]. Our aim in writing this paper is to fill this gap. Although our method is not limited to stochastic

[†]Division of Applied Mathematics, Brown University, Providence, RI 02912, USA

[‡]Pacific Northwest National Laboratory, Richland, WA 99352, USA

[§]Department of Applied Mathematics and Statistics, University of California Santa Cruz, Santa Cruz, CA 95064, USA

[¶]george_karniadakis@brown.edu

Diffusion	$N(x,t,u;\omega) = \nabla a(x;\omega)\cdot\nabla u + a(x;\omega)\nabla^2 u$
Advection	$N(x,t,u;\omega) = \dfrac{\partial u}{\partial t} + V(x;\omega)\nabla u$
Advection-Reaction	$N(x,t,u;\omega) = \dfrac{\partial u}{\partial t} + V(x)\nabla u - k(x;\omega)(1-u^2)$

TABLE 1.1
Examples of nonlinear operators defining the initial/boundary value problem (1.1).

PDEs with global solution trajectories, we begin the discussion of our new methods by considering the following model

$$\begin{cases} N(x,t,u(x,t;\omega);\omega) = f(x,t;\omega), & x\in\mathcal{D} \\ B(u(x,t;\omega)) = g(x,t;\omega), & x\in\partial\mathcal{D}\ , \\ C(u(x,t_0;\omega)) = z(x;\omega), & x\in\mathcal{D} \end{cases} \tag{1.1}$$

where $\mathcal{D}\subseteq\mathbb{R}^d$ is a bounded spatial domain with boundary $\partial\mathcal{D}$, N is a nonlinear operator, B is a boundary operator, C is an initial condition operator and ω is an element of the sample space. We assume that the initial/boundary value problem (1.1) is well posed for each realization of the random forcing $f(x,t;\omega)$, random boundary conditions $g(x,t;\omega)$ and random initial condition $z(x;\omega)$. Examples of N are given in Table 1.1. Note that we are considering both time-dependent as well as time-independent problems. In the latter case the initial condition operator is obviously not needed. We decompose $\mathcal{D}$ into a set of P subdomains $\{\mathcal{D}_1,...,\mathcal{D}_P\}$ such that

$$\overline{\mathcal{D}} = \bigcup_{i=1}^{P}\overline{\mathcal{D}}_i, \qquad \overline{\mathcal{D}}_i = D_i\cup\partial\mathcal{D}_i. \tag{1.2}$$

A classical Schwarz method to compute the solution to the SPDE (1.1) in a *covering* of $\mathcal{D}$ is summarized in Algorithm 1. At each iteration and at each time step we solve (in a predetermined sequence) P restricted stochastic PDE systems in the form

$$\begin{cases} N_i(x,t,u_i^n(x,t;\omega);\omega) = f_i(x,t;\omega), & x\in\mathcal{D}_i \\ B(u_i^n(x,t;\omega)) = g(x,t;\omega), & x\in\partial\mathcal{D}_i\setminus\Gamma_i\ , \\ B(u_i^n(x,t;\omega)) = \widetilde{g}_i(x,t;\omega), & x\in\Gamma_i \end{cases} \tag{1.3}$$

where $u_i^n(x,t;\omega)$ denotes the solution in $\mathcal{D}_i$ at the n-th iteration, Γ_i is the boundary of $\mathcal{D}_i$ lying in the interior of $\mathcal{D}$, while N_i and f_i are, respectively, the restrictions of N and f to $\mathcal{D}_i$. The *artificial boundary conditions* $\widetilde{g}_i$ on Γ_i are determined by the stochastic solution from the previous iteration.

The first step in solving the sequence of local stochastic PDEs (1.3) relies in representing their solution appropriately. This is crucial in stochastic domain decomposition, as local stochastic expansions usually do not preserve multi-point statistical properties across different domains. If we follow a naive approach, we can simply discretize (1.1), e.g., by using of probabilistic collocation [10, 11, 28], polynomial chaos [8, 48, 50], or reduced basis methods [7], and then apply Algorithm 1 to

```
begin
    n = 1;
    initialize {u_i^0}_{i=1}^P at random;
    while ||u^{n-1} − u^n||_{x∈D} > ε do
        for 1 ≤ i ≤ P do
            solve the restricted PDE system (1.3) on D_i;
        end
        n = n + 1;
    end
end
```

Algorithm 1: Classical domain decomposition method with overlapping domains.

each solution sample of (1.1). Although this process can be effectively parallelized [6], it does not exploit the possibly low-dimensional structure of the stochastic solution within each subdomain $\mathcal{D}_i$. Such low-dimensionality, as we will see, is a consequence of the finite correlation length of the solution field.

Our object is to develop new stochastic domain decomposition (SDD) algorithms by imposing *proper* transmission boundary conditions between heterogeneous stochastic domains and stochastic systems. The starting point is to construct a representation of the stochastic solution in each domain $\mathcal{D}_i$ that preserves global statistical properties. This topic is discussed in detail in the next section 2 that leverages on *local* low-dimensionality. In section 3 we propose two new SDD algorithms that seek coupling across the interfaces in a weak sense: the first one enforces the continuity of the conditional mean and the variance of the solution across adjacent subdomains by using Schwarz iterations. The second one simultaneously interfaces multiple functionals of the stochastic solution, such as the first few statistical moments, through PDE-constrained optimization. In section 4 we apply the proposed algorithms to different stochastic problems. Specifically, we consider stochastic elliptic problems, stochastically advected scalar fields and nonlinear advection-reaction problems. For each system we perform systematic convergence studies. The main results are then summarized and discussed in section 5. We also include an appendix in which we prove convergence of the local expansion method discussed in section 2.

2. Embedding Random Processes. In this section we consider the problem of embedding a random process or a random field defined on a domain $\mathcal{D}$ into a set of subdomains $\mathcal{D}_i \subseteq \mathcal{D}$. By "embedding" here we mean representing the solution locally in such a way that prescribed statistical properties are preserved across different subdomains. This has advantages in terms of dimensionality if the process has a finite correlation length, as the local representation usually involves a reduced number of random variables. Consequently, the stochastic problem (1.1) can be reduced, at least in principle, to a sequence of local stochastic problems in each $\mathcal{D}_i$ of smaller dimension. A major challenge when embedding globally defined processes and fields in a set of subdomains is the preservation of global statistical properties. Indeed, we cannot expect that, in general, the two- or three-point correlation functions are preserved across different subdomains. This is a serious issue, since such multi-point statistics are often key elements of the stochastic solution. In other words, if the domain decomposition is not done appropriately in terms of local expansions and suitable stochastic interface conditions, we may introduce a systematic error when computing the solution to (1.1) through the system (1.3).

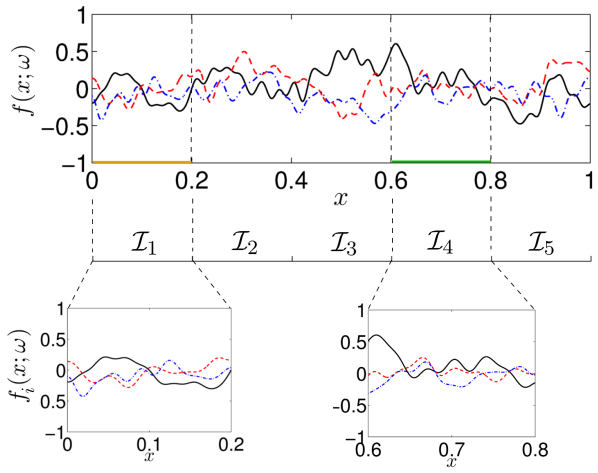

FIG. 2.1. *Embedding a stochastic process with finite correlation length into a non-overlapping covering of* $[0,1]$*: the restriction of the process* $f(x;\omega)$ *to each subdomain* $\mathcal{I}_i$ *yields a subprocess* $f_i(x;\omega)$ *that can be represented in terms of a smaller number of random variables.*

2.1. Local Expansions. Let us consider a random function $f(x;\omega)$, $x \in \mathcal{D}$ with given mean and covariance

$$\bar{f}(x) = \langle f(x;\omega) \rangle , \qquad C(x,y) = \langle f(x;\omega) f(y;\omega) \rangle - \langle f(x;\omega) \rangle \langle f(y;\omega) \rangle . \tag{2.1}$$

Given a decomposition of $\mathcal{D}$ in terms of P overlapping subdomains $\{\mathcal{D}_1, ..., \mathcal{D}_P\}$, we would like to represent $f(x;\omega)$ locally in each subdomain $\mathcal{D}_i$, in such a way that the two-point statistical properties are preserved, even when computed across different subdomains. In particular, let us assume that the correlation length of $f(x;\omega)$ is relatively short, compared to the characteristic length of $\mathcal{D}$. Then, it is reasonable to assume that the restriction of $f(x;\omega)$ to $\mathcal{D}_i$ is statistically correlated only with the restriction of $f(x;\omega)$ to the neighboring subdomains, say $\mathcal{D}_{i-1}$ and $\mathcal{D}_{i+1}$ in a one-dimensional setting. This allows us to represent $f(x;\omega)$ in $\mathcal{D}_i$ by using a set of random variables that are shared only among adjacent subdomains.

To this end, we introduce a new set of subdomains $\{\mathcal{I}_1, ..., \mathcal{I}_{P'}\}$ to propagate the correlation structure of $f(x;\omega)$ across different $\mathcal{D}_i$. For instance, if $\mathcal{D}_i$ and $\mathcal{D}_{i+1}$ are adjacent and the correlation length of $f(x;\omega)$ is smaller than both $|\mathcal{D}_i|$ and $|\mathcal{D}_{i+1}|$, then we could define the subdomain $\mathcal{I}_{i+1} \subset \mathcal{D}_i \cup \mathcal{D}_{i+1}$. In this way, the restriction of $f(x;\omega)$ to $\mathcal{I}_{i+1}$ allows us to propagate the correlation structure of $f(x;\omega)$ from $\mathcal{D}_i$ to $\mathcal{D}_{i+1}$. It is important to remark that the random process $f(x;\omega)$ is first represented locally on the new subdomains $\{\mathcal{I}_1, ..., \mathcal{I}_{P'}\}$, then later redistributed on $\{\mathcal{D}_1, ..., \mathcal{D}_P\}$ to obtain the solution of the stochastic problem. In general, $\{\mathcal{I}_i\}$ is different from $\{\mathcal{D}_i\}$. However, if the local processes on each $\mathcal{D}_i$ are statistically independent, then we can take $\mathcal{I}_i = \mathcal{D}_i$. The method can be thought of as a *two-level* domain decomposition, in which each level represents a decomposition of $\mathcal{D}$, e.g., $\{\mathcal{D}_i\}$ and $\{\mathcal{I}_i\}$. The procedure is sketched in Fig. 2.2 for $P \geq 3$ and Fig. 2.3 for $P = 2$. In general, however, when solving (1.1) we allow for a *multi-level* domain decomposition, e.g., each level corresponding to multi-correlated stochastic processes with different scales. The

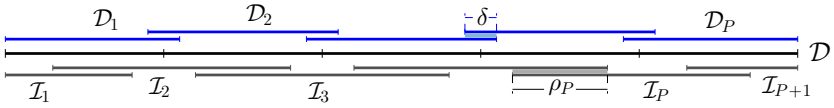

FIG. 2.2. *One-dimensional domain decomposition with overlapping subdomains. Shown are the subdomains* $\{\mathcal{D}_i\}$ *used to compute the solution to* (1.1) *and the subdomains* $\{\mathcal{I}_i\}$ *used to represent the external random forcing* f.

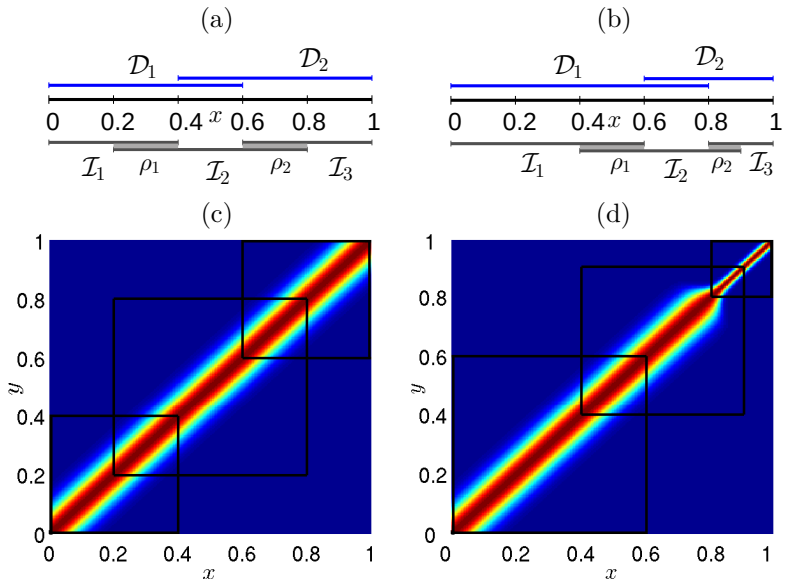

FIG. 2.3. *One-dimensional domain decomposition of* $[0,1]$ *into two overlapping domains* $\{\mathcal{D}_1, \mathcal{D}_2\}$ *and three expansion intervals* $\{\mathcal{I}_1, \mathcal{I}_2, \mathcal{I}_3\}$ *(Figs. (a) and (b)). In Figs. (c) and (d) we show how* $\{\mathcal{I}_1, \mathcal{I}_2, \mathcal{I}_3\}$ *partition the domain of a Gaussian covariance function with constant correlation length* $l_c = 0.08$ *(Fig. (c)) and variable correlation length ranging from* 0.08 *to* 0.02 *(Fig. (d)). In both cases, the overlap* ρ_i *between* $\mathcal{I}_i$ *and* $\mathcal{I}_{i+1}$ *is chosen to be larger than the largest correlation length in* $\mathcal{I}_i \cap \mathcal{I}_{i+1}$.

overlap between the subdomains $\{\mathcal{I}_1, ..., \mathcal{I}_{P'}\}$

$$\Delta_i \stackrel{\text{def}}{=} \mathcal{I}_i \cap \mathcal{I}_{i+1}, \qquad \rho_i \stackrel{\text{def}}{=} |\Delta_i|$$

should be chosen to be larger than the correlation length of $f(x;\omega)$ (see appendix A for the error analysis). In the presence of multi-correlated random processes [4] we can define a domain decomposition for each process.

2.1.1. A One-Dimensional Example. With reference to Fig. 2.2, let us consider two overlapping coverings of $\mathcal{D}$, $\{\mathcal{I}_1, ..., \mathcal{I}_{P+1}\}$ and $\{\mathcal{D}_1, ..., \mathcal{D}_P\}$ in which $\mathcal{D}_i$ and $\mathcal{D}_{i+1}$ share the same local representation of $f(x;\omega)$ in $\mathcal{I}_{i+1}$. We first compute the Karhunen-Loève (K-L) expansion of $f(x;\omega)$ on the i-th subdomain $\mathcal{I}_i$. To this end, we simply restrict the covariance function (2.1) to $\mathcal{I}_i$ and solve the well-known K-L eigenvalue problem [4, 41, 42]. We denote $C_i(x,y)$ as the local covariance function on $\mathcal{I}_i \times \mathcal{I}_i$. In order to ensure that the local expansions preserve the global statistical properties on the overlapping subdomains, i.e., $C(x,y) = \sum_{i=1}^{P+1} C_i(x,y)\mathbf{1}_{\mathcal{I}_i \times \mathcal{I}_i}$,

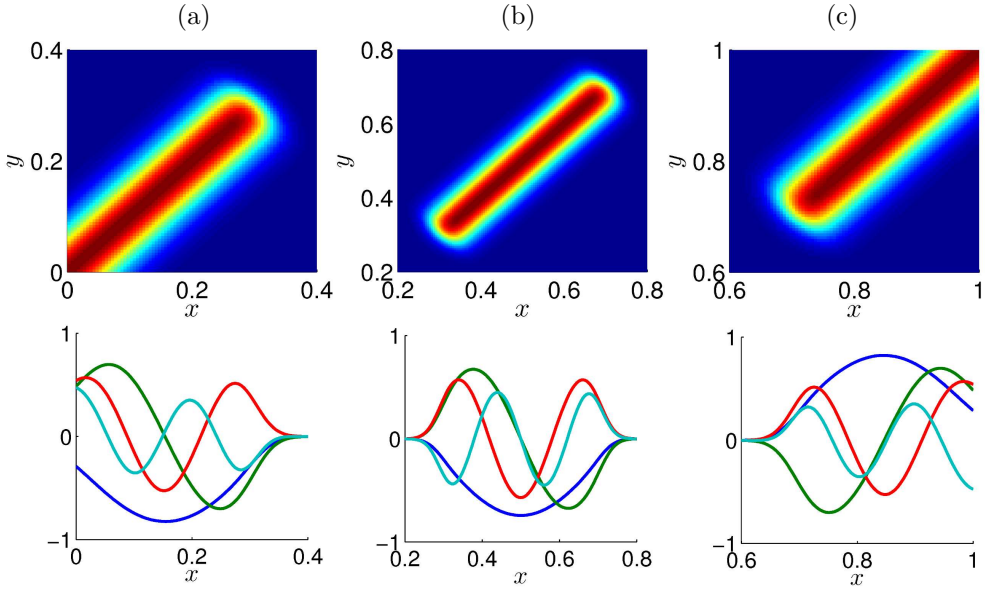

FIG. 2.4. *Filtered local covariance functions* (2.3) *over three expansion intervals as in Fig. 2.3(c) and corresponding first four K-L eigenfunctions. The overlap region is set to* $\rho_1 = \rho_2 = 0.2$.

$C_i(x,y)$ is smoothly filtered to zero on the overlapping region $\Delta_i \times \Delta_i$ and the adjacent $C_{i+1}(x,y)$ takes the counterpart that remains after subtracting the filtered covariance from the global one. In order words, we define a filter $\mathcal{F}_i$ such that

$$\mathcal{F}_i[C_i(x,y)] = \begin{cases} C_i(x,y), & (x,y) \in (\mathcal{I}_i \times \mathcal{I}_i) \backslash (\Delta_i \times \Delta_i), \\ C_i(x,y)\mathfrak{f}(x,y), & (x,y) \in \Delta_i \times \Delta_i, \end{cases} \tag{2.2}$$

where $\mathfrak{f}(x,y)$ is a smooth function (e.g., a Gaussian or an arctan function) that decays from one to zero toward the boundary of $\mathcal{I}_i$, and $\mathcal{F}_i = 0$ elsewhere on $(\mathcal{I}_i \times \mathcal{I}_i)^c$. This allows us to define the following *filtered local covariances*

$$\begin{cases} \hat{C}_1(x,y) = \mathcal{F}_1[C(x,y)], & (x,y) \in \mathcal{I}_1 \times \mathcal{I}_1, \\ \hat{C}_i(x,y) = \mathcal{F}_i[C(x,y) - \hat{C}_{i-1}(x,y)], & (x,y) \in \mathcal{I}_i \times \mathcal{I}_i, \quad (i = 2, ..., P) \\ \hat{C}_{P+1}(x,y) = C(x,y) - \hat{C}_P(x,y), & (x,y) \in \mathcal{I}_{P+1} \times \mathcal{I}_{P+1}, \end{cases} \tag{2.3}$$

We comment that any continuously decreasing function with the denoted boundary condition can be used for the filter, since the summation of the local covariance will still be $C(x,y)$. However, the smoothness of the filter, i.e., the regularity of $\mathcal{F}_i[C_i(x,y)]$, will affect the number of terms in the local K-L expansion. As an example, in Fig. 2.4 we apply the arctan filter to the Gaussian covariance function shown in Fig. 2.3 (c). It can be easily verified that

$$C(x,y) = \sum_{i=1}^{P+1} \hat{C}_i(x,y) \mathbf{1}_{\mathcal{I}_i \times \mathcal{I}_i}, \qquad (x,y) \in \mathcal{D} \times \mathcal{D}, \tag{2.4}$$

i.e., the global covariance function $C(x,y)$ can be represented as a summation of filtered local covariances $\hat{C}_i(x,y)$. Now, the local K-L expansion of $f(x;\omega)$ on $\mathcal{I}_i$ can

be computed by using the local covariance function $\hat{C}_i(x,y)$ as

$$f_i(x;\omega) = \sum_{m=1}^{\infty} \sqrt{\lambda_{i,m}} e_{i,m}(x)\xi_{i,m}(\omega), \quad x \in \mathcal{I}_i, \tag{2.5}$$

where $\lambda_{i,m}$ and $e_{i,m}(x)$ are eigenvalues and (normalized) eigenfunctions of the integral equation

$$\int_{\mathcal{I}_i} \hat{C}_i(x,\, y) e_{i,m}(x) dx = \lambda_{i,m} e_{i,m}(y).$$

The (uncorrelated) random variables $\xi_{i,m}(\omega)$ can be obtained through projection as

$$\xi_{i,m}(\omega) = \frac{1}{\sqrt{\lambda_{i,m}}} \int_{\mathcal{I}_i} f_i(x;\omega) e_{i,m}(x) dx.$$

Finally, the approximation of the random function $f(x;\omega)$ can be written as a summation of truncated K-L expansions in each $\mathcal{I}_i$, i.e.,

$$f_M(x;\omega) \overset{\text{def}}{=} \sum_{i=1}^{P+1} \left(\sum_{m=1}^{M_i} \sqrt{\lambda_{i,m}} e_{i,m}(x) \mathbf{1}_{\mathcal{I}_i} \xi_{m,i}(\omega) \right), \quad x \in \mathcal{D}, \tag{2.6}$$

where M_i is chosen to achieve a prescribed level of accuracy in each $\mathcal{I}_i$. Here is where the finite correlation length of $f(x;\omega)$ comes in. In fact, the number of random variables M_i strongly depends on how much we "zoom-in" (with $\mathcal{I}_i$) into the graph of $C(x,y)$. The series expansion (2.6) allows us to solve the stochastic problem (1.1) by using domain decomposition. In a one-dimensional setting the solution in each subdomain $\mathcal{D}_i$ depends only on $(M_i + M_{i+1})$ random variables, which is usually much smaller that the number of random variables arising from the global K-L expansion. Also, $\mathcal{D}_i$ shares M_i and M_{i+1} random variables with its adjacent domains $\mathcal{D}_{i-1}$ and $\mathcal{D}_{i+1}$, respectively.

3. Interfacing Subdomains. The choice of the interface condition between different subdomains is an *open question* in stochastic domain decomposition methods. No rigorous theory has yet been developed for interfaces defined in terms of *functionals* of a stochastic field, e.g., mean, variance or multi-point correlations, although this is of fundamental importance when propagating uncertainty across subdomains. Interfacing the whole stochastic field, e.g., through Monte Carlo or sparse collocation approaches [6, 7] is prohibitively expensive, since the interface operator has to be applied to each sample. On the other hand, if we interface only *low-dimensional functionals* of the stochastic solution, e.g., few statistical moments, then we obtain a tremendous reduction in computational cost at the expense of a possible accuracy loss. In this section we propose two new SDD algorithms that exploit the basic idea of interfacing only low-dimensional functionals of the solution in different subdomains. Specifically, the first algorithm uses an interface condition defined in terms of a set of *conditional moments* (section 3.1). The second algorithm, on the other hand, simultaneously interfaces multiple functionals of the stochastic solution, such as the first few statistical moments, by using *PDE-constrained optimization* (section 3.2). The accuracy of both methods is assessed numerically in section 4.

3.1. Conditional Moment Interface Method. Our first SDD algorithm is based on interfacing moments or cumulants of the stochastic solution across different subdomains by using Schwarz iterations. Schwarz methods are well-established for deterministic problems, and convergence results can be found in several books [20, 32, 35, 40] and reviews [52, 53]. In particular, it has been found that the convergence rate of classical algorithms is rather slow and very much dependent on the extent of overlap between different subdomains. To overcome these drawbacks, new classes of Schwarz methods were proposed in recent years, e.g., optimized Schwarz methods. These new algorithms are based on a more effective transmission of information at interfaces between subdomains. For instance, Robin-Robin conditions [14] and conditions expressed in terms on *non-local* operators [5, 12, 13, 17] can yield convergence without overlap.

The conditional moment interface method we propose in this section imposes the interface condition between different subdomains $\mathcal{D}_i$ by using the statistical moments. These are easily computed by using the random variables of the local K-L expansion in the overlapping region $\mathcal{I}_i$ between different subdomains. If we denote by $\boldsymbol{\xi}_i = (\xi_{i,1}, \cdots, \xi_{i,M_i})$ such random variables, then the conditional average of the solution can be expressed as

$$\langle\, u(x,t;\boldsymbol{\xi}_i,\boldsymbol{\xi}_j)|\,\boldsymbol{\xi}_i\rangle \stackrel{\text{def}}{=} \int u(x,t;\boldsymbol{\xi}_i,\boldsymbol{\xi}_j)p(\boldsymbol{\xi}_j|\boldsymbol{\xi}_i)d\boldsymbol{\xi}_j,$$

where $p(\boldsymbol{\xi}_j|\boldsymbol{\xi}_i)$ is the conditional probability density of $\boldsymbol{\xi}_j$ given $\boldsymbol{\xi}_i$. The *artificial boundary condition* $\widetilde{g}_i$ in the system (1.3) can be selected by imposing the conservation of the k-th conditional moment*

$$\mu_k(\,B(u_i^n(x,t;\boldsymbol{\xi}_i,\boldsymbol{\xi}_{i+1}))|\,\boldsymbol{\xi}_j) = \mu_k(\widetilde{g}_i(x,t;\omega)|\,\boldsymbol{\xi}_j), \qquad x\in\Gamma_i, \quad j=i \text{ or } i+1, \tag{3.1}$$

where

$$\mu_k(u|\boldsymbol{\xi}_j) = \begin{cases} \langle u|\boldsymbol{\xi}_j\rangle\,, & k=1,\\ \big\langle (u-\langle u|\boldsymbol{\xi}_j\rangle)^k|\boldsymbol{\xi}_j\big\rangle\,, & k>1, \end{cases} \tag{3.2}$$

Unfortunately, this condition (3.1) alone does not allow us to determine $\widetilde{g}_i$ uniquely, due to the uncommon random variables, i.e., the complement of $\boldsymbol{\xi}_j$. A simple choice among multiple boundary conditions is to impose the same conditional mean for fixed $\boldsymbol{\xi}_i$ over all collocation points of $\boldsymbol{\xi}_{i+1}$, i.e.,

$$\widetilde{g}(x,t;\boldsymbol{\xi}_i,\,\cdot\,) = \big\langle u_{i-1}^n(x,t;\boldsymbol{\xi}_{i-1},\boldsymbol{\xi}_i)\big\rangle_{i-1}. \tag{3.3}$$

Obviously, this satisfies Eq. (3.1) for $k=1$. However, when implemented in (1.3) the scheme dissipates excessively the variance at the boundaries, since the variance with respect to $\boldsymbol{\xi}_{i+1}$ is imposed to be zero. In order to mitigate this effect and achieve a better accuracy for higher-order moments we propose hereafter several corrections. To this end, let us first introduce the *mean-shifted boundary condition*, which basically imposes continuity of the mean solution across different subdomains. This can be expressed by the following boundary condition

$$\begin{aligned}\widetilde{g}_i^n[1](x,t;\boldsymbol{\xi}_i,\boldsymbol{\xi}_{i+1}) \stackrel{\text{def}}{=} u_i^n(x,t;\boldsymbol{\xi}_i,\boldsymbol{\xi}_{i+1}) - \langle u_i^n(x,t;\boldsymbol{\xi}_i,\boldsymbol{\xi}_{i+1})\rangle_{i+1}\\ +\big\langle u_{i-1}^n(x,t;\boldsymbol{\xi}_{i-1},\boldsymbol{\xi}_i)\big\rangle_{i-1}.\end{aligned} \tag{3.4}$$

*In practice, we use the marginal expectation $\langle u(x,t;\boldsymbol{\xi}_i,\boldsymbol{\xi}_j)\rangle_j \stackrel{\text{def}}{=} \int u(x,t;\boldsymbol{\xi}_i,\boldsymbol{\xi}_j)p(\boldsymbol{\xi}_i,\boldsymbol{\xi}_j)d\boldsymbol{\xi}_j$ that appears after multiplying the conditional average with $p(\boldsymbol{\xi}_i)$.

Note that (3.4) satisfies Eq. (3.1) for $k = 1$, and at the same time it does not affect the variance of the solution within the subdomain D_i. This overcomes the variance dissipation problem arising from the simpler boundary condition (3.3). A further improvement of the interface condition can be obtained by using second-order statistical properties. We shall call the corresponding boundary condition as *variance scaling boundary condition*. Specifically, we set

$$\widetilde{g}_i^n[2](x,t;\boldsymbol{\xi}_i,\boldsymbol{\xi}_{i+1}) \overset{\text{def}}{=} \left(u_i^n(x,t;\boldsymbol{\xi}_i,\boldsymbol{\xi}_{i+1}) - \langle u_i^n(x,t;\boldsymbol{\xi}_i,\boldsymbol{\xi}_{i+1})\rangle_{i+1}\right)\frac{\sigma_{i-1}(u_{i-1}^n)}{\sigma_{i+1}(u_i^n)} + \left\langle u_{i-1}^n(x,t;\boldsymbol{\xi}_{i-1},\boldsymbol{\xi}_i)\right\rangle_{i-1}, \tag{3.5}$$

where $\sigma_j(u)$ is defined by

$$\sigma_j(u(x,t;\omega)) \overset{\text{def}}{=} \left[\left\langle u(x,t;\omega)^2\right\rangle_j - \langle u(x,t;\omega)\rangle_j^2\right]^{1/2}.$$

Note that (3.5) satisfies Eq. (3.1) for both $k = 1$ and 2, but it may lead to unstable Schwarz iterations due to the division by $\sigma_j(u)$. To avoid such instabilities, we combine (3.4) and (3.5) into one scheme. This yields the conditional moment interface Algorithm 2, in which for simplicity we have considered only two domains $\mathcal{D}_1$ and $\mathcal{D}_2$ (three expansion intervals $\mathcal{I}_1$, $\mathcal{I}_2$ and $\mathcal{I}_3$; see Fig. 2.3). The boundary conditions appearing in the algorithm are explicitly given as

$$\begin{aligned}
\widetilde{g}_r^n[1](x,t;\omega) &= u_1^n(x,t;\boldsymbol{\xi}_1,\boldsymbol{\xi}_2) - \langle u_1^n(x,t;\boldsymbol{\xi}_1,\boldsymbol{\xi}_2)\rangle_1 + \left\langle u_2^{n-1}(x;\boldsymbol{\xi}_2,\boldsymbol{\xi}_3)\right\rangle_3,\\
\widetilde{g}_r^n[2](x,t;\omega) &= \left(u_1^n(x,t;\boldsymbol{\xi}_1,\boldsymbol{\xi}_2) - \langle u_1^n(x,t;\boldsymbol{\xi}_1,\boldsymbol{\xi}_2)\rangle_1\right)\frac{\sigma_3(u_2^{n-1})}{\sigma_1(u_1^n)} + \langle u_1^n(x,t;\boldsymbol{\xi}_1,\boldsymbol{\xi}_2)\rangle_3,\\
\widetilde{g}_l^n[1](x,t;\omega) &= \widetilde{g}_2^n[1](x,t;\boldsymbol{\xi}_2,\boldsymbol{\xi}_3),\\
\widetilde{g}_l^n[2](x,t;\omega) &= \widetilde{g}_2^n[2](x,t;\boldsymbol{\xi}_2,\boldsymbol{\xi}_3).
\end{aligned}$$

We initialize the iterative sequence by using the mean boundary condition (3.4), and iterate until a prescribed tolerance ϵ is achieved on the residual

$$r = \frac{\|u^n(x,t;\omega) - u^{n-1}(x,t;\omega)\|_{x\in\mathcal{D}}}{\|u^{n-1}(x,t;\omega)\|_{x\in\mathcal{D}}}.$$

We call n^* the transition iteration for which $r < \epsilon$, and denote the computed boundary condition as $\widetilde{g}_i^{n^*}[1](x,t;\boldsymbol{\xi}_i,\boldsymbol{\xi}_{i+1})$. After the transition iteration, we switch the boundary condition to the following weighted one

$$\widetilde{g}_i^n(x,t;\boldsymbol{\xi}_i,\boldsymbol{\xi}_{i+1}) = w\widetilde{g}_i^{n^*}[1](x,t;\boldsymbol{\xi}_i,\boldsymbol{\xi}_{i+1}) + (1-w)\widetilde{g}_i^n[2](x,t;\boldsymbol{\xi}_i,\boldsymbol{\xi}_{i+1}), \tag{3.6}$$

where $w \in [0,1]$ is the weight between the converged solution from the mean shifting boundary condition and the new solution from variance scaling approach. Note that the condition (3.6) is equivalent to the mean shifting condition (3.4) in the limit $w \to 1$.

Analytical convergence of the proposed iterative algorithm is an open question at this point. Still, we emphasize that the local solutions correspond to the exact random excitation from the original system (1.1), and the boundary conditions (3.4)-(3.6) impose continuity in the first few moments of the solution. In particular, it takes advantage of the local expansions developed in section 2 that attain the exact global covariance structure while providing a set of common random variables among

begin
  $n = 1$
  initialize $\{u_i^0\}_{i=1}^2$ at random
  take the local boundary condition $\widetilde{g}_r^n \equiv \widetilde{g}_r^n[1]$ and $\widetilde{g}_l^n \equiv \widetilde{g}_l^n[1]$ **while** $\|u^{n-1} - u^n\|_{x\in\mathcal{D}} > \varepsilon$ *or* $\|u_1^n - u_2^n\|_{x\in\mathcal{D}_1\cap\mathcal{D}_2} > \bar{\varepsilon}$ **do**
    solve

$$\begin{aligned} N_1(x,t,u_1^n(x,t;\omega);\omega) &= f_1(x,t;\omega), \qquad x\in\mathcal{D}_1 \\ B(u_1^n(x,t;\omega)) &= g(x,t;\omega), \qquad x\in\partial\mathcal{D}_1\setminus\Gamma_1. \\ B(u_1^n(x,t;\omega)) &= \widetilde{g}_r^n(x,t;\omega), \qquad x\in\Gamma_1 \end{aligned}$$

$$\begin{aligned} N_2(x,t,u_2^n(x,t;\omega);\omega) &= f_2(x,t;\omega), \qquad x\in\mathcal{D}_2 \\ B(u_2^n(x,t;\omega)) &= g(x,t;\omega), \qquad x\in\partial\mathcal{D}_2\setminus\Gamma_2. \\ B(u_2^n(x,t;\omega)) &= \widetilde{g}_l^n(x,t;\omega), \qquad x\in\Gamma_2 \end{aligned}$$

    if $\|u^{n-1} - u^n\|_{x\in\mathcal{D}} > \epsilon\|u^{n-1}\|_{x\in\mathcal{D}}$ **then**
      $n^* = n$
    else
      $\widetilde{g}_r^n \equiv w\widetilde{g}_r^{n*}[1] + (1-w)\widetilde{g}_r^n[2]$,
      $\widetilde{g}_l^n \equiv w\widetilde{g}_l^{n*}[1] + (1-w)\widetilde{g}_l^n[2]$.
    end

    $n = n + 1$
  end
end

Algorithm 2: Conditional moment interface method.

the adjacent subdomains. Thus, continuity can be imposed strongly on the shared random space along with matching up to the second-order moments on the remaining variables. In case of locally independent stochastic excitation, i.e., $\mathcal{I}_i = \mathcal{D}_i$, where the subdomains do not share a common random space, the conditional moment in the boundary condition becomes a regular moment. Still, rigorous analysis will be the subject of our future work, and a recent study in [3] proposes a guideline of the error contribution concerning local polynomial chaos expansions.

3.2. PDE-Constrained Interface Method. The conditional moment interface method discussed in the previous section can be reformulated as a *PDE-constrained optimization* problem:

$$\min_{\widetilde{\boldsymbol{g}}} \mathcal{J}(\widetilde{\boldsymbol{g}}) \qquad \text{s.t.} \qquad \text{Eq. (1.3)}, \tag{3.7}$$

where $\widetilde{\boldsymbol{g}} = (\widetilde{g}_1, \widetilde{g}_2, \cdots, \widetilde{g}_P) = (\widetilde{g}(x|_{\Gamma_1}, t;\omega), \widetilde{g}(x|_{\Gamma_2}, t;\omega), \cdots, \widetilde{g}(x|_{\Gamma_P}, t;\omega))$,

$$\begin{aligned} \mathcal{J}(\tilde{\boldsymbol{g}}) = \sum_{i=1}^{P-1}\sum_{k=1}^{R} &\Big\| \mu_k(u_i(x,t;\widetilde{g}_i,\omega)\mathbf{1}_{\Gamma_{i+1}\cap\mathcal{D}_i})|\boldsymbol{\xi}_{i+1}\big) - \mu_k(\widetilde{g}_{i+1}|\,\boldsymbol{\xi}_{i+1})\Big\| \\ &+ \Big\|\mu_k(\,u_{i+1}(x,t;\widetilde{g}_{i+1},\omega)^k\mathbf{1}_{\Gamma_i\cap\mathcal{D}_{i+1}}|\,\boldsymbol{\xi}_{i+1}) - \mu_k(\widetilde{g}_i|\,\boldsymbol{\xi}_{i+1})\Big\|\,, \end{aligned} \tag{3.8}$$

defined as in Eq. (3.2). Clearly, if u is the exact solution to Eq. (1.1) then $\mathcal{J} = 0$. Within this framework, Algorithm 2 can be considered as an iterative approach to

solve the optimization problem (3.7) with $R = 2$. Intuitively, the choice of R depends on the statistical information we are willing to keep. For example, if we select $R = 1$ in (3.8) then (3.7) is expected to yield results similar to the conditional moment interface method with the mean-shifted boundary condition.

Within the optimization framework it is rather easy to define *generalized interface conditions* between the random solution in different subdomains. To this end, we simply need to specify a suitable objective function $\mathcal{J}$ (or a set of functions) to be minimized. Suppose, for example, that we are interested in preserving the first R statistical moments of the solution across different domains. In this case we can consider

$$\mathcal{J}(\tilde{\boldsymbol{g}}) = \sum_{i=1}^{P-1}\sum_{k=1}^{R} \|\mu_k(u_i(x,t;\tilde{g}_i,\omega)\mathbf{1}_{\mathcal{D}_i\cap\mathcal{D}_{i+1}}) - \mu_k(u_{i+1}(x,t;\tilde{g}_{i+1},\omega)\mathbf{1}_{\mathcal{D}_i\cap\mathcal{D}_{i+1}})\|_2, \tag{3.9}$$

where $\|\cdot\|_2$ is the L^2 norm on the physical space, and μ_k is defined as

$$\mu_k(u) = \begin{cases} \langle u \rangle, & k = 1, \\ \left\langle (u - \langle u \rangle)^k \right\rangle, & k > 1. \end{cases} \tag{3.10}$$

The main difference between (3.8) and (3.9) is that we replaced conditional moments with moments. With this new objective function, we can solve the PDE-constrained optimization problem (3.7) to obtain the boundary conditions $\tilde{\boldsymbol{g}}$, hence determining the global solution u. The optimization problem (3.7) can also be split into a sequence of local problems, e.g., involving only few domains $\mathcal{D}_i$ at a time. For example we could consider

$$\min_{\widetilde{g}_1} \mathcal{J}_1(\widetilde{g}_1), \quad \min_{\widetilde{g}_2} \mathcal{J}_2(\widetilde{g}_2), \quad \cdots, \quad \min_{\widetilde{g}_P} \mathcal{J}_2(\widetilde{g}_P) \qquad \text{s.t.} \qquad \text{Eq. (1.3)}, \tag{3.11}$$

and solve the *multi-objective optimization problem* by using, e.g., computational game theory [33,36]. In this framework each objective function $\mathcal{J}_i$ is considered as a player in a game. Each player tries to minimize his objective iteratively in a cooperative (Stackelberg games [47]) or a non-cooperative (Nash games [27]) setting. We refer to [33,36] for additional details.

In each subdomain $\mathcal{D}_i$ the solution u_i is determined by $f_i, \tilde{g}_i$ and N_i (see Eq. (1.3)). Therefore, for a given f_i and N_i, the stochastic solver in each $\mathcal{D}_i$ can be represented by the mapping

$$F_i : \tilde{g}_i \mapsto u_i.$$

At this point, we expand $\tilde{g}_i(x,t;\omega)$ in a polynomial chaos basis $\psi_{im}(x;\omega)$

$$\tilde{g}_i(x,t;\omega) = \sum_{m=1}^{Q_i} c_{i,m}(t)\psi_{i,m}(x;\omega), \tag{3.12}$$

and rewrite Eq. (3.9) as

$$\begin{aligned} \mathcal{J}(\boldsymbol{c}_1, \boldsymbol{c}_2, \cdots, \boldsymbol{c}_P) = \sum_{i=1}^{P-1}\sum_{k=1}^{R} \|&\mu_k(u_i(x,t;\boldsymbol{c}_i)\mathbf{1}_{\mathcal{D}_i\cap\mathcal{D}_{i+1}}) \\ &-\mu_k(u_{i+1}(x,t;\boldsymbol{c}_{i+1})\mathbf{1}_{\mathcal{D}_i\cap\mathcal{D}_{i+1}})\|_2, \end{aligned} \tag{3.13}$$

begin

initialize $\boldsymbol{c}_i$ with the results of deterministic problem;

prepare SPDE solver in each subdomain $\mathcal{D}_i$, i.e., set the mapping $F^\dagger : \boldsymbol{c}_i \mapsto u_i$;

set the objective function $\mathcal{J}(\boldsymbol{c}_1, \boldsymbol{c}_2, \cdots, \boldsymbol{c}_P)$ in (3.14) and choose appropriate weights w_k defining the norm, if necessary;

solve the optimization problem $\min \mathcal{J}(\boldsymbol{c}_1, \boldsymbol{c}_2, \cdots, \boldsymbol{c}_P)$ subject to Eq. (1.3).

end

Algorithm 3: PDE-constrained interface method.

where $\boldsymbol{c}_i(t) = (c_{i,1}, c_{i,2}, \cdots, c_{i,Q_i})$. Note that in this way we built a new mapping representing the stochastic solver in each subdomain $\mathcal{D}_i$

$$F^\dagger : \boldsymbol{c}_i \mapsto u_i.$$

We conclude this section by emphasizing that the objective function (3.9) can also take a weighted form

$$\mathcal{J}(\tilde{\boldsymbol{g}}) = \sum_{i=1}^{P-1} \sum_{k=1}^{R} w_k \|\mu_k(u_i(x,t;\tilde{g}_i)\mathbf{1}_{\mathcal{D}_i \cap \mathcal{D}_{i+1}}) - \mu_k(u_{i+1}(x,t;\tilde{g}_{i+1})\mathbf{1}_{\mathcal{D}_i \cap \mathcal{D}_{i+1}})\|_2, \tag{3.14}$$

to account for possible different magnitudes in the statistical moments or cumulants. The SPDE-constrained optimization method is summarized in Algorithm 3.

3.3. Comparison between the Conditional Moment and the PDE Constrained Interface Methods. The conditional moment interface method enforces the continuity of the conditional mean and variance of the solution across adjacent subdomains by using Schwarz iterations. In particular, by representing the correlation structure in terms of shared random variables, the algorithm allows us to perform convergent iterations. On the other hand, the PDE-constrained method provides a general framework to perform domain decomposition on stochastic PDEs. In practice, it allows us to set quite general interface conditions by minimizing suitable functionals of the random solution. The algorithm does not leverage on shared random variables across adjacent domains as before, but it performs a full PDE-constrained optimization in terms of moments or cumulants. This can be considered as an extension of well-known techniques for deterministic PDE [2, 16, 29].

4. Numerical Results. In this section we compare the performances of our SDD algorithms in numerical examples involving linear and nonlinear stochastic PDEs. Specifically, we consider elliptic problems with random diffusion coefficients, randomly advected scalar fields, and nonlinear advection-reaction problems with random reaction rate. The governing equations are summarized in Table 1.1.

4.1. Stochastic Elliptic Problem. Let us consider the stochastic elliptic problem

$$-\frac{d}{dx}\left(a(x;\omega)\frac{du(x;\omega)}{dx}\right) = \sin(2\pi x), \qquad u(0;\omega) = u(1;\omega) = 0, \qquad x \in [0,1], \tag{4.1}$$

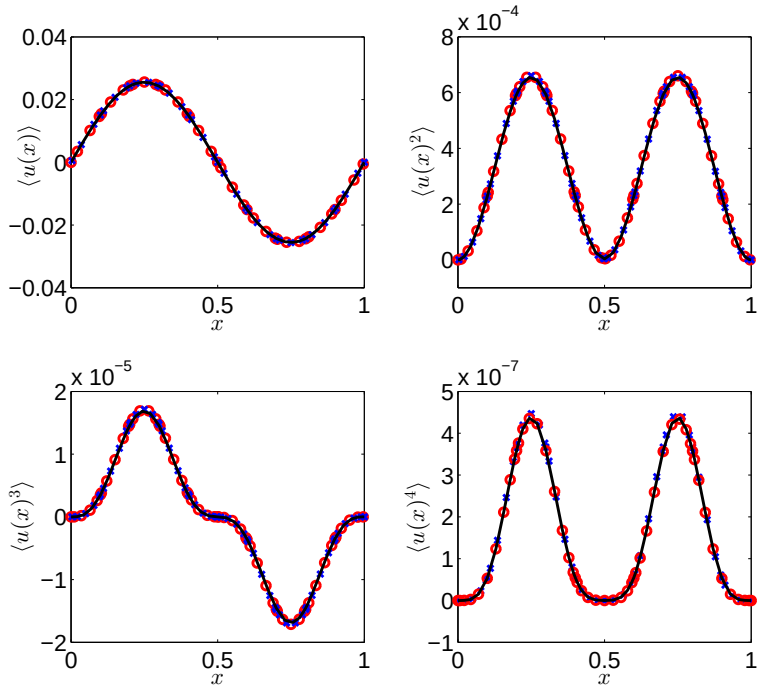

FIG. 4.1. *Stochastic elliptic problem. Statistical moments of the solution for random diffusion coefficients with variable correlation length. Reference solution (black line); Results from the conditional moment interface method (SDD-M) (red circles) and the PDE-constrained interface method (blue ×). It is seen that the solution computed by the proposed SSD algorithms is accurate.*

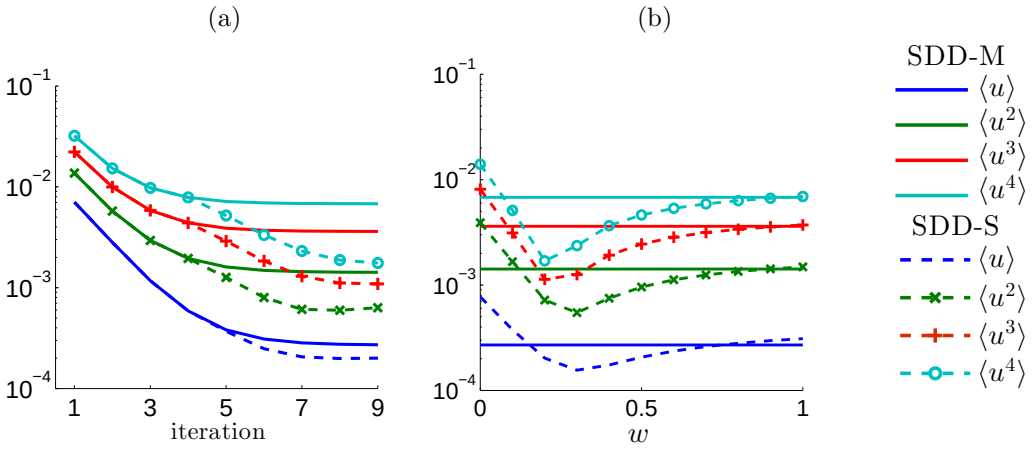

FIG. 4.2. *Stochastic elliptic problem. (a) Relative L_2 error in the first four moments as computed by the conditional mean (SDD-M) and conditional standard deviation (SDD-S) algorithms with $w = 0.2$ and $\epsilon = 10^{-3}$. (b) Relative error versus the weight w for fixed $\epsilon = 10^{-4}$. It is seen that the SDD-S algorithm improves the accuracy in computing higher-order statistical moments near $w = 0.2$.*

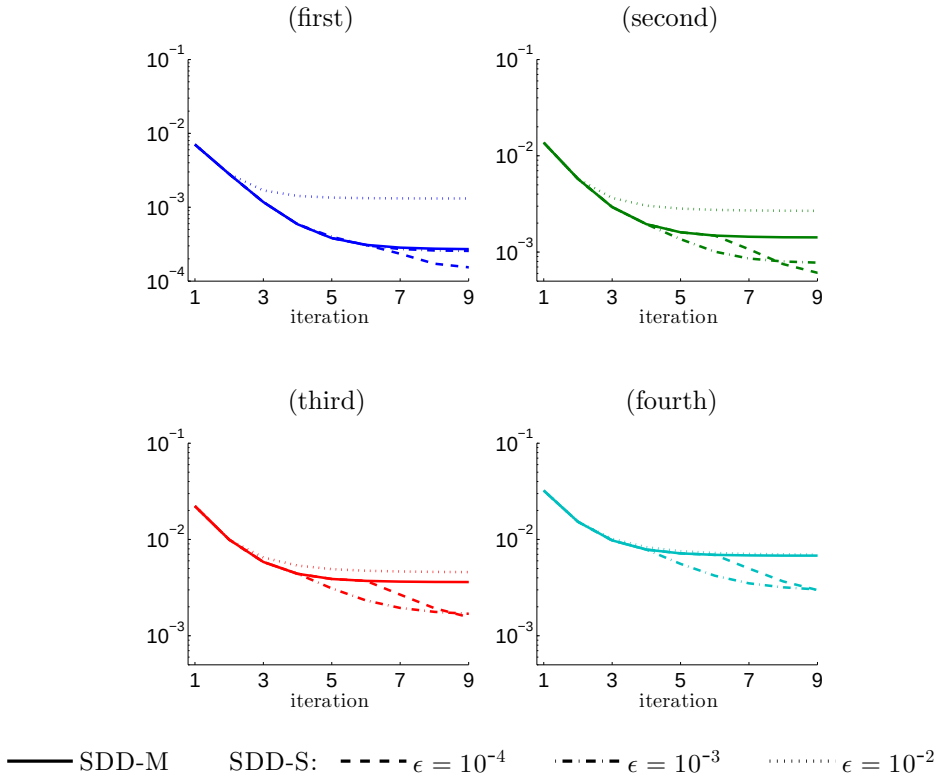

FIG. 4.3. *Stochastic elliptic problem. Relative L_2 error in the first four moments for different transition thresholds ϵ. The threshold determines the accuracy and number of iteration for convergence, hence, it must be selected by taking into account the target error level.*

where the diffusion coefficient $a(x;\omega)$ is assumed to be a random process with mean and covariance function

$$\langle a(x;\omega)\rangle = 1, \qquad \mathrm{Cov}\{a(x;\omega), a(y;\omega)\} = \sigma_a^2 \exp\left[-\frac{|x-y|^2}{l_c^2}\right]. \tag{4.2}$$

We will study processes with constant as well as variable correlation lengths l_c (see Fig. 2.3(c,d)). The prototype stochastic problem (4.1) has been studied with many different techniques, e.g., Wick-Malliavin approximations [46], stochastic collocation [1], polynomial chaos [50] and domain decomposition methods [6, 7]. The latter approach was shown to be effective and massively parallel, but it did not exploit the fundamental relation between the correlation length of the random diffusivity and the domain decomposition of (4.1).

Hereafter we demonstrate computational advantages of such low-dimensional representation. To this end, we consider an overlapping covering of the spatial domain $[0, 1]$ in terms of two subdomains $\{\mathcal{D}_1, \mathcal{D}_2\}$. By using the local K-L expansion method we discussed in section 2, we embed the random function $a(x;\omega)$ into the set of subdomains $\mathcal{I}_i$ shown in Fig. 2.3(a,b). This yields a set of sub-processes in the form (2.5), which allow us to construct *local* reduced-order stochastic representations of $a(x;\omega)$ preserving second-order statistical properties (see the Appendix A). Specifically, we assume that the random variables $\boldsymbol{\xi}_i(\omega)$ in (2.5) are uniform on $[-1, 1]$, and

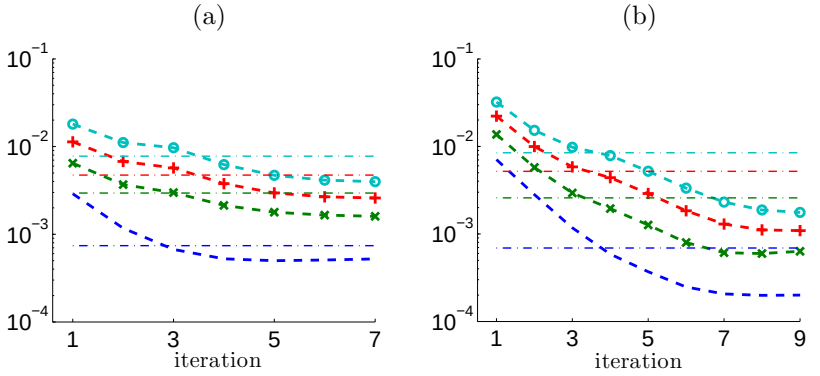

FIG. 4.4. *Stochastic elliptic problem. Comparison between the relative L_2 errors of the SDD-S method (−−) and the PDE-constrained method (−·−) for constant $l_c = 0.08$ (Fig. (a)) and variable l_c (Fig. (b)). It is seen that the SDD-M method is more accurate than the PDE-constrained method.*

error in $\langle u^k \rangle$	$k=1$	$k=2$	$k=3$	$k=4$
Conditional moment method	2.9514e-04	1.0076e-03	1.7654e-03	2.8584e-03
PDE-constrained method	7.4173e-04	2.9523e-03	4.7312e-03	7.7749e-03

TABLE 4.1

Stochastic elliptic problem. Relative L_2 errors in the first four statistical moments and the standard deviation of the solution computed by using the conditional moment and the PDE-constrained interface methods.

that $\sigma_a = 0.2$ in (4.2). The dimensionality in the random space reduces from 12 to 9 in each subdomain for the constant correlation case, and from 17 to 12 and 13 for the other case, where the K-L expansion is truncated to achieve 95% eigen-spectrum. The solution on $\mathcal{D}_i$ can be written as $u_i(x;\omega) = u_i(x;\boldsymbol{\xi}_i(\omega),\boldsymbol{\xi}_{i+1}(\omega))$, where $\boldsymbol{\xi}_2(\omega)$ are the random variables shared between the subdomains $\mathcal{D}_1$ and $\mathcal{D}_2$. The whole spatial domain $\mathcal{D}$ is discretized by using 10 spectral elements of order 10, and we consider a probabilistic collocation method for the random variables $\boldsymbol{\xi}_i$.

In Fig. 4.1 we compare the first four moments computed by the global K-L and the decomposed K-L expansion for random diffusion coefficients $a(x;\omega)$ with variable correlation length. The domain decomposed solution is computed by using the SDD algorithm with mean boundary condition (SDD-M) - Eq. (3.4). We found that although we are interfacing the subdomain $\mathcal{D}_1$ and $\mathcal{D}_2$ only through the conditional mean field, the decomposed solution basically coincides with the global one just after few iterations. Specifically, the results of Fig. 4.1 are obtained at the fourth iteration.

Convergence of SDD with mean shifted boundary condition (3.4) (SDD-M) and with variance scaling boundary condition (3.6) (SDD-S) is demonstrated in Fig. 4.2. It is seen that the L_2 error in the fourth moment, which is the largest one, becomes smaller than 1% after the third iteration. Also, the SDD-S method is more accurate than SDD-M. We also performed convergence studies in terms of other parameters appearing in the SDD-S method, in particular the transition threshold ϵ and w. The results are summarized in Fig. 4.2(b) and Fig. 4.3. In particular, in Fig. 4.2(b) we plot the L_2 error of the SDD solution versus w for fixed $\epsilon = 10^{-4}$. It is seen that there

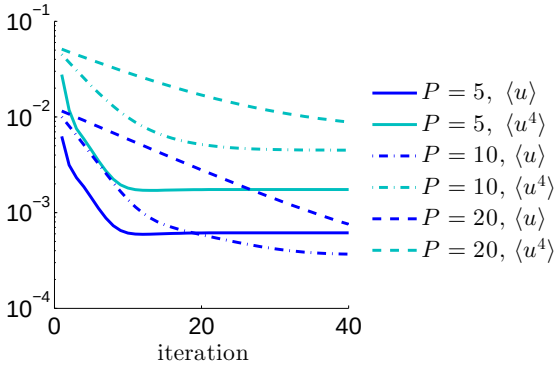

FIG. 4.5. *Stochastic elliptic problem. Relative L_2 error in the first- and fourth-order moment versus the iteration number in SDD-M method. Shown are results for different numbers of subdomains P.*

P	1	5	10	20
$\|\mathcal{I}_i\|$	1	0.2	0.1	0.05
M_i	119	23	12	6

TABLE 4.2
Stochastic elliptic problem. Length of $\mathcal{I}_i$ and number of random variables M_i in the local K-L expansion within each $\mathcal{I}_i$ as a function of the total number of subdomains P. Here M_i is determined by setting a threshold of 5% in the error of the second order moment computed by the truncated K-L series.

exist an optimal value of w near $w = 0.2$, which coincides with the ratio between the noise amplitude σ_a and the mean. Note also that in the limit $w \to 1$ the error of SDD-S coincides with SDD-M (see section 3.1).

The effects of the transition threshold on the convergence of the Schwarz iterations is studied in Fig. 4.3 for $\epsilon = 10^{-2}$, 10^{-3}, and 10^{-4}. In particular, we found that the solution computed with smaller ϵ is more accurate but it exhibits a slower convergence rate. Thus, the parameter ϵ determines *both* accuracy and convergence of Schwarz iterations. The errors obtained by using $\epsilon = 10^{-2}$ are the largest ones, but still bounded by 10^{-2}. In Table 4.1 and Fig. 4.4 we compare the relative L_2 errors obtained by using the conditional moment and PDE-constrained interface methods with $R = 2$ and $w_k = 1$. Specially, we consider the problem (4.1) with random diffusion coefficient of correlation length $l_c = 0.08$. In all cases, it is seen that the conditional moment interface method is more accurate than the PDE-constrained interface method. The computational cost of both methods is discussed in section 5.

4.1.1. Extension to Multiple Subdomains. So far we considered only two overlapping domains $\mathcal{D}_1$ and $\mathcal{D}_2$ to compute the solution to (4.1). We now extend the SDD algorithms to multiple subdomains $\{\mathcal{D}_1, ..., \mathcal{D}_P\}$ and $\{\mathcal{I}_1, ..., \mathcal{I}_{P+1}\}$, with $P = 5$, 10 or 20. In particular, we set

$$\mathcal{D}_i = [x_{i-1} - \delta', x_i + \delta'], \qquad \mathcal{I}_{i+1} = [x_{i-1} + \rho', x_{i+1} - \rho'], \tag{4.3}$$

where $\{x_i\}_{i=0}^P$ are points in $[0,1]$, while δ' and ρ' are positive numbers determining the extent of overlap between subdomains (see Fig. 2.2). When $\{x_i\}_{i=0}^P$ are uniformly spaced, with spacing $\triangle x$ (i.e., $x_i = i\triangle x$), the overlapping region is $\delta = |\mathcal{D}_i \cap \mathcal{D}_{i+1}| = 2\delta'$ and $\rho = |\mathcal{I}_i \cap \mathcal{I}_{i+1}| = \triangle x - 2\rho'$. The length of the expansion intervals $2\triangle x$ and the overlapping length ρ should be selected by taking into account the correlation length of the diffusion coefficient, here set to $l_c = 0.008$. Thus, we choose δ' and ρ' in order to obtain $\rho = 0.04$, 0.04, and 0.03 for $P = 5$, 10, and 20, respectively. Thanks to the finite correlation length of the diffusion coefficient, we have that the number of terms in the local K-L expansion decreases significantly when we increase the number of subdomains (see Table 4.2). This allows us to solve a sequence of local low-dimensional problems when performing Schwarz iterations.

Convergence of the SDD-M algorithm with multiple subdomains is shown in Fig. 4.5, where we plot the relative L_2 error of the first- and fourth-order moment. Note that as the number of subdomains increases to $P = 20$, the convergence rate deteriorates due to errors in the local K-L expansion. This can be improved by setting a tighter threshold for the K-L truncation error (see Appendix A). We do not apply Algorithm 3 to solve this problem because the number of variables in the objective function is too large for $P = 20$. Indeed this yields a high-dimensional global optimization problem (3.7) requiring specifically designed algorithms to be solved. An alternative way to proceed is to split the objective function into several functions and consider multi-objective optimization, e.g., based on computational game theory. An advantage of using this approach relies on the fact that the high-dimensional optimization problem can be split into a sequence of low-dimensional ones. The global minimizer is constructed in an alternating-direction setting, e.g., by solving each local optimization problem independently and then iterate on the subsequent ones.

4.2. Stochastic Advection. Next, we consider the stochastic advection problem

$$\frac{\partial u(x,t)}{\partial t} = -a(x;\omega)\frac{\partial u(x,t)}{\partial x}, \qquad x \in [0,1], \quad t \geq 0, \tag{4.4}$$

with initial condition $u(x,0) = \sin(2\pi x)$. The mean velocity is set to $\langle a(x;\omega)\rangle = 1/(2\pi)$ and the covariance function is assumed to be as in Eq. (4.2) with $\sigma_a = 1/(10\pi)$. We consider both Gaussian covariances shown in Fig. 2.3(c,d), i.e., with constant and variable correlation lengths, and represent $a(x;\omega)$ by using the local K-L we discussed in section 2 decomposed into the two subdomains as shown in Fig. 2.3(a,b). Regarding the boundary conditions, we set periodic boundary conditions $u(0) = u(1)$ for the case where $a(x;\omega)$ has constant correlation length, and a Dirichlet condition $u(0) = \sin(-t)$ for variable correlation lengths. In Fig. 4.6 we plot the first four moments of the solution to (4.4) as computed by the SDD-S and the PDE-constrained interface methods, for the case where $a(x;\omega)$ has constant correlation length $l_c = 0.08$. Here we set $\epsilon = 10^{-2}$ and $w = 0.1$ in the SDD-S algorithm. It is seen that both methods yield accurate statistical moment up to $t = 1.0$ (see also Fig. 4.8). In Fig. 4.7 we study the standard deviation of the solution at $t = 0.5$, for advection velocities with variable and constant correlation lengths. In the latter case, Fig. 4.7(b), we see that the SDD-S algorithm provides more accurate results than SDD-M, by preserving the periodicity of the standard deviation. In this test, we notice that the difference between the errors of two methods is very small when t is small, and the PDE-constrained method is more accurate for the problem with periodic boundary conditions.

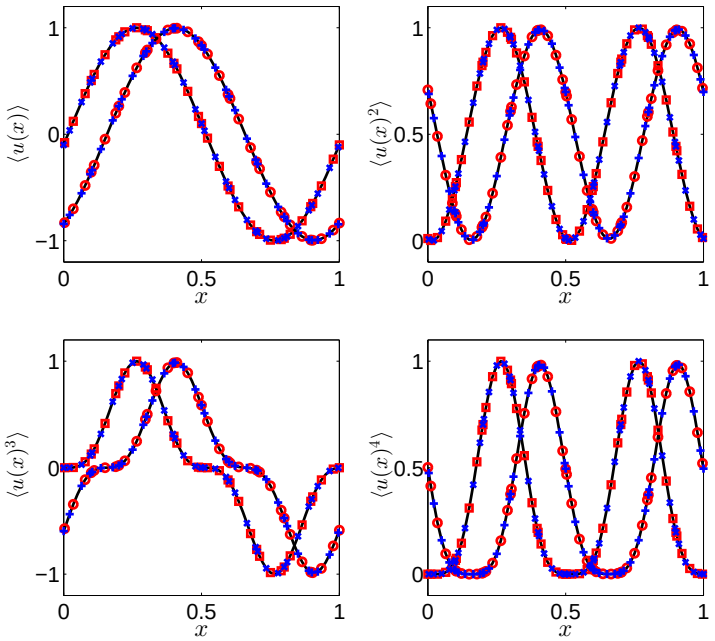

FIG. 4.6. *Stochastic advection problem. First four statistical moments. The reference solution (black line) is compared with the SDD-S method (red line) and the PDE-constrained interface method (blue line) at two different times:* $t = 0.1$ *(red square, blue ×) and* $t = 1.0$ *(red circle, blue +).*

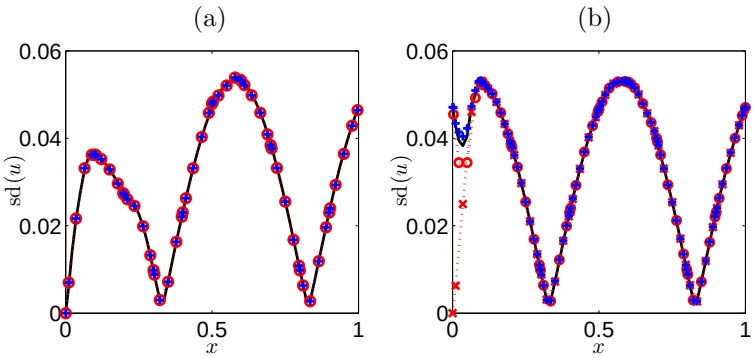

FIG. 4.7. *Stochastic advection problem. Standard deviation of the solution at* $t = 0.5$*. The reference solution (black line) is compared with the results obtained by using the conditional moment interface methods: SDD-M (red ×), SDD-S (red o) and the PDE-constrained method (blue +). In particular, in Fig. (a) we study the case where the random advection velocity has a variable correlation length ranging from* 0.02 *to* 0.08*. Results for the case of constant correlation length are shown in Fig. (b).*

4.3. Stochastic Advection-Reaction. In this last example we consider an advection-reaction problem with nonlinear reaction term and stochastic reaction rate

$$\frac{\partial u}{\partial t} = V(x)\frac{\partial u}{\partial x} + \left(k_0(x) + \sigma_k k_1(x;\omega)\right) R(u), \tag{4.5}$$

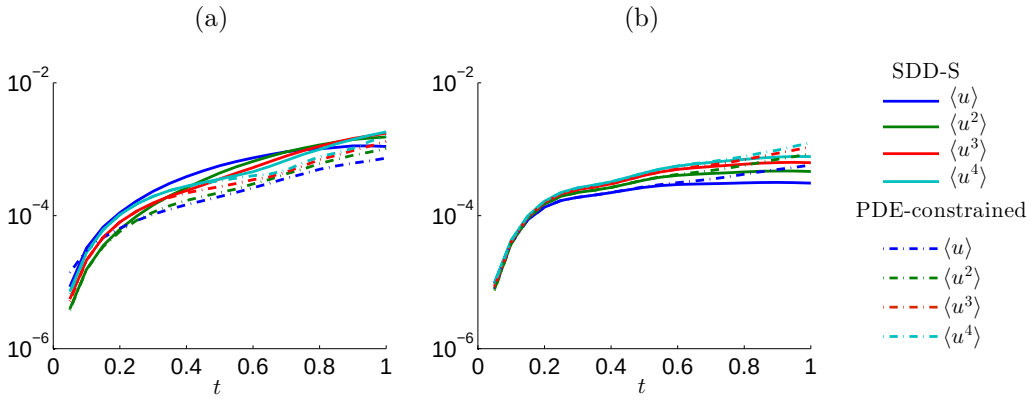

FIG. 4.8. *Stochastic advection problem. Relative L_2 errors in the first four statistical moments of the solution versus time. We show results computed by using the SDD-S (−) and the PDE-constrained (− · −) interface methods for the cases of constant correlation length ($l_c = 0.08$) and periodic boundary conditions (Fig. (a)), and variable correlation length ranging from* 0.08 *to* 0.02 *and Dirichlet boundary condition (Fig. (b)).*

where

$$V(x) = -\frac{1}{2}\left(1 + e^{(\sin(2\pi x)+\cos(2\pi x))/2} - \cos(2\pi x)\right),$$
$$k_0(x) = 1 - \frac{2}{5}\left(e^{-\sin(2\pi x)/2} + \cos(2\pi x)\right),$$

$\sigma_k = 0.2$, $R(u) = 1-u^2$, with initial condition $u_0(x) = \sin(2\pi x)$ and periodic boundary conditions. This problem was studied in [43] by using the Mori-Zwanzig projection operator method (see also [38,44]). The perturbation in the reaction rate, $k_1(x;\omega)$, is modeled as a Gaussian random field with Gaussian covariance function and correlation length varying from 0.08 to 0.02 (see Fig. 2.3(d)). The results of our simulations by using two subdomains as in the previous section are shown in Fig. 4.9, where we plot the first four moments of the stochastic solution at different times obtained by using the SDD-M and PDE-constrained interface methods. The relative L_2 error of such moments is plotted in Fig. 4.10 versus time. It is seen that the SDD-M method is more accurate than the PDE-constrained method. Both algorithms produce the same error slope in time.

In addition, we consider a random reaction rate with a Gaussian covariance kernel having correlation length $l_c = 0.008$, and compute the solution by using the SDD algorithm on multiple subdomains as in section 4.1.1. We take the subdomains $\{\mathcal{D}_i\}$ and $\{\mathcal{I}_i\}$ defined as in (4.3) for $P = 5$, 10, and 20. The dimensionality of the random space associated with this decomposition is shown in Table 4.2. The relative L_2 errors in the first four statistical moments are plotted in Fig. 4.11 for $P = 5$ and $P = 20$. Although the errors slightly increase as we divide the domain into smaller subdomains, the accuracy does not depend strongly on P. In particular, Fig. 4.11(b) plots the error with respect to P, which shows that the error stays in the same order of magnitude. Thus, we observe that the convergence of the SSD method depends less on the number of subdomains for this problem than the Poisson equation in section 4.1.1.

5. Summary. In this paper we proposed new stochastic domain decomposition methods for multi-scale propagation of uncertainty in heterogeneous stochastic sys-

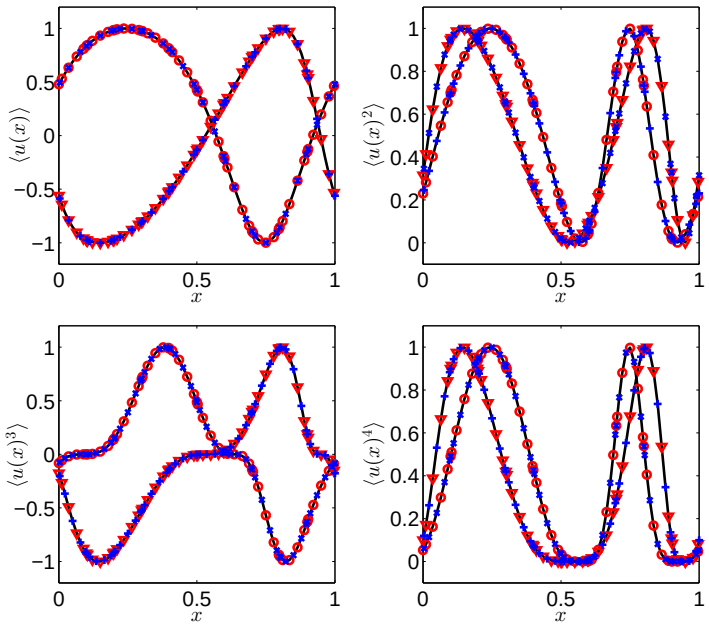

FIG. 4.9. *Stochastic advection-reaction problem. First four statistical moments of the solution to the advection reaction equation* (4.5) *with correlation length that varies from 0.02 to 0.08. The reference solution (black line) is compared with the SDD-M method (red line) and the PDE-constrained interface method (blue line) at two different times:* $t = 0.5$ *(red triangle, blue +) and* $t = 1.0$ *(red circle, blue x).*

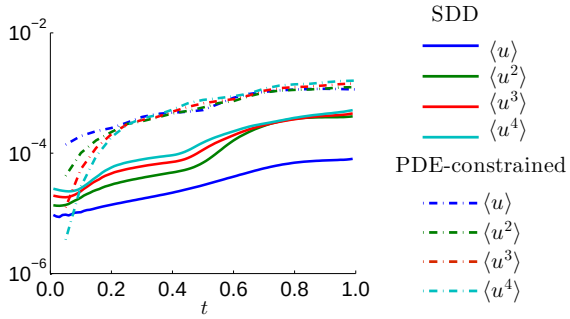

FIG. 4.10. *Stochastic advection-reaction problem. Relative* L_2 *errors in the first four statistical moments of the solution to the the stochastic advection reaction problem* (4.5) *versus time. We show results computed by using the moment interface SDD-M (−) and the PDE-constrained (− · −) methods for the case of variable correlation length decomposed into two subdomains.*

tems. The key idea relies on new types of interface conditions between different subdomains combined with reduced-order local representations of random processes and fields. This allows us to reduce the stochastic problem to a sequence of problems of smaller stochastic dimension, while properly propagating uncertainty across domains. We proposed two new algorithms for this purpose, based on conditional moments (section 3.1), and PDE-constrained optimization (section 3.2). In both cases, the interface conditions are defined by *low-dimensional functionals* of the stochastic solution (e.g., moments or cumulants). We emphasize that no rigorous theory has yet

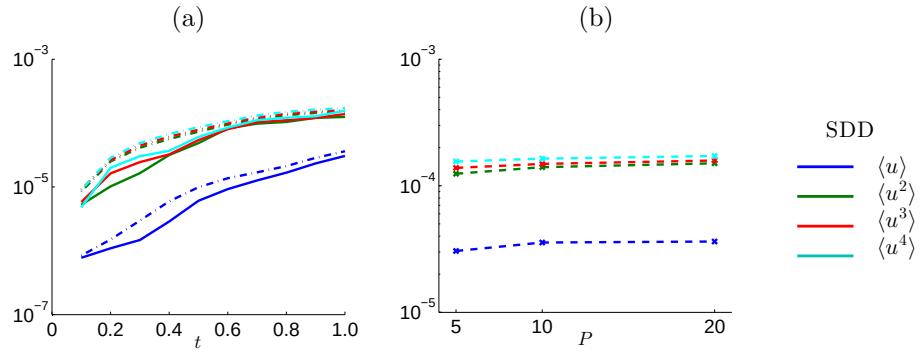

FIG. 4.11. *Stochastic advection-reaction problem. Relative L_2 errors in the first four statistical moments versus time (a) by using $P = 5$ $(-)$ and $P = 20$ $(- \cdot -)$ number of subdomains. Fig. (b) plots the error versus P at time $t = 1$ which shows that the error does not depend strongly on P.*

Conditional moment method	PDE-constrained method
$C_{det}\left(\frac{N}{P}\right) \cdot C(M) \cdot n_{itr} \cdot P$	$C_{det}\left(\frac{N}{P}\right) \cdot C(M) \cdot C_{opt}(M,P) \cdot P$

TABLE 5.1

Comparison between the computational cost of the conditional moment and the PDE-constrained interface methods. Here C_{det} is the cost of the deterministic solver on a single subdomain, $C(M)$ is the number of (sparse grid) collocation points, n_{itr} is the Schwarz iteration number, and C_{opt} counts the number of deterministic solves in the PDE-constrained optimization. In our simulations, $C_{opt} \sim \mathcal{O}(10^2)$ while n_{itr} is usually less than 10. In these cases the PDE-constrained method is more costly.

been developed for stochastic systems with interfaces defined in terms of *functionals* of the stochastic field. However, the numerical tests we performed in section 4, demonstrate that the SDD methods proposed here are relatively accurate and efficient for both linear and nonlinear problems. The computational cost of the new algorithms is summarized in Table 5.1. In particular, the conditional moment interface method requires a deterministic solve at each Schwarz iteration within each subdomain. This has to be multiplied by the number of (sparse grid) collocation points we use to represent the parametric input uncertainty. On the other hand, the computational cost of the PDE-constrained method is proportional to C_{opt} times the cost of a deterministic solve, where C_{opt} in our examples is of the same order of magnitude as the number of gPC coefficients in the local polynomial chaos expansions i.e., $\mathcal{O}(10^2)$. Hence, in our examples the PDE-constrained method is more costly, since $n_{itr} < 10^2$.

There are interesting connections between the conditional moment and the PDE-constrained methods. In particular, the conditional moment method can be seen as an algorithm to solve a special type of PDE-constrained optimization problem. In future work we will exploit this connection further. Although, our methods impose the interface condition in a weak sense that does not guarantee sample-wise continuity of the solution, we emphasize the applicability of our methods to systems without global description of the random field, e.g., atomistic to continuum coupling problems, and particularly the PDE-constrained method can be considered as an extension of deterministic optimization-based coupling methods [30, 31]. Another interesting research direction is the localized optimization approach based on computational game theory

mentioned in section 3.2. In such framework, each objective function is considered as a player which tries to minimize his value in a cooperative (Stackelberg games [47]) or a non-cooperative (Nash games [27]) way. In this setting, local optimization can be used in connection with the conditional moment approach to develop a *predictor-corrector* scheme. We will also extend the conditional moment method to interfaces defined by higher-order moments. This can be done, e.g., by using non-normal transformation techniques [9].

Summary:

1. The conditional moment method is more accurate than the PDE-constrained method and it is computationally more efficient for a large number of subdomains. This is particularly true for nonlinear problems.
2. The PDE-constrained method allows us to couple stochastic simulations with generalized interface conditions, and it is applicable regardless of the structure of the random solution. The computational efficiency of the method can be enhanced by splitting the global optimization problem into local ones and then using multi-objective optimization.
3. Both conditional moment and PDE-constrained algorithms can be parallelized.

In future work, we will extend the proposed algorithms to stochastic systems with hybrid coupling, e.g., stochastic particle simulations coupled with stochastic PDEs and embedded multi-dimensional domains. In addition, analytical study of our iterative scheme will be in the subject of our future work. A recent study in [3] proposes a method of analysis concerning a local polynomial chaos expansion. However global trajectories should be available, which is not usually possible for the problem we consider here.

Acknowledgments. We would like to thank Dr. Jared Knap of ARL for stimulating discussions and useful suggestions. We also would like to thank Prof. Xiaoliang Wan of LSU for pointing out important aspects of the optimization approach to domain decomposition. This work was supported by ARO grant W911NF-14-1-0425, AFOSR grant FA9550-14-1-0212, ARL grant W911NF-12-2-0023.

Appendix A. Convergence Analysis of the Local K-L Expansions. In this section we prove that the local expansion method introduced in section 2, preserves the two-point correlation function of the field across different subdomains. To this end, let us compute the error in representing the global covariance function in terms of local expansions, i.e.,

$$\left\| C(x,y) - \sum_{i=1}^{P+1} \hat{C}_i(x,y) \mathbf{1}^{(x,y)}_{\mathcal{I}_i \times \mathcal{I}_i} \right\| = \left\| C(x,y) \mathbf{1}^{(x,y)}_{\cap_i (\mathcal{I}_i \times \mathcal{I}_i)^c} \right\| \leq O(\varepsilon_C). \tag{A.1}$$

Here ε_C is an upper bound of $C(x,y)$ on $\cap_i (\mathcal{I}_i \times \mathcal{I}_i)^c$ which depends on the length of the subdomains and the overlapping region. The convergence of the local K-L expansion is given by the usual K-L theorem, provided that the filtered covariance function $\hat{C}_i(x,y)$ is smooth and positive semi-definite. In fact, the L_2 error is obtained as

$$\varepsilon_i^2 \overset{\text{def}}{=} \int_{\mathcal{I}_i} \left\langle \left(f_i(x;\omega) - \sum_{m=1}^{M_i} \sqrt{\lambda_{m,i}} e_{m,i}(x) \xi_{m,i}(\omega) \right)^2 \right\rangle dx = \sum_{M_i+1}^{\infty} \lambda_{m,i}, \tag{A.2}$$

so that each series can be truncated according to the error of the local eigenspectrum. An upper bound for the error in the covariance function is obtained as

$$\begin{aligned}\|C(x,y) - \langle f_M(x;\omega) f_M(y;\omega)\rangle\| &\leq \left\| C(x,y) - \sum_{i=1}^{P+1} \hat{C}_i(x,y) \mathbf{1}^{(x,y)}_{\mathcal{I}_i\times\mathcal{I}_i} \right\| \\ &+ \left\| \sum_{i=1}^{P+1} \hat{C}_i(x,y) \mathbf{1}^{(x,y)}_{\mathcal{I}_i\times\mathcal{I}_i} - \left(\sum_{i=1}^{P+1} \sum_{m=1}^{M_i} \lambda_{m,i} e_{m,i}(x) e_{m,i}(y) \mathbf{1}^{(x,y)}_{\mathcal{I}_i\times\mathcal{I}_i} \right) \right\| \\ \leq \left\| C(x,y) \mathbf{1}^{(x,y)}_{\cap_i (\mathcal{I}_i\times\mathcal{I}_i)^c} \right\| &+ \left\| \sum_{i=1}^{P+1} \left(\hat{C}_i(x,y) - \sum_{m=1}^{M_i} \lambda_{m,i} e_{m,i}(x) e_{m,i}(y) \right) \mathbf{1}^{(x,y)}_{\mathcal{I}_i\times\mathcal{I}_i} \right\| \\ &\leq O(\varepsilon_C) + \sum_{i=1}^{P+1} O(\varepsilon_i).\end{aligned}$$

The first part is due to domain decomposition while the second part is due to the truncation of the local expansions (see Fig. A.1(c,d) that plots the errors related to these quantities). If $\mathcal{D}$ is bounded and $C_i(x,y)$ are positive semi-definite, both ε_C and ε_i go to zero. This is demonstrated numerically in Fig. A.1(a), where we plot the error in the covariance function as the number of subdomains P increases. In particular, the covariance function of $f(x;\omega)$ is chosen to be Gaussian with correlation length $l_c = 0.008$. Compared to the global K-L expansion ($P = 1$), the decomposed K-L expansion converges much faster in each subdomain as we increase P. This is due to the fact that the relative correlation length of the process becomes larger when we "zoom-in" with the domain decomposition (see Fig. 2.1). This implies that the local K-L expansion requires a smaller number of random variables (m) to achieve the same level of accuracy. In Fig. A.1(b) we plot the relative error on the entire domain $\mathcal{D}$ versus the total number of random variables, i.e., $m \cdot P$, Note that the global K-L expansion gives a lower bound for the errors, since it is the optimal representation of the process on $\mathcal{D}$. We also observe that the total number of random variables to achieve the same level of accuracy increases as we increase P.

REFERENCES

[1] I. Babuska, F. Nobile, and R. Tempone. A stochastic collocation method for elliptic partial differential equations with random input data. *SIAM J. Numer. Anal.*, 45(3):1005–1034, 2007.

[2] P. B. Bochev and D. Ridzal. An optimization-based approach for the design of PDE solution algorithm. *SIAM J. Numer. Anal*, 47(51):3938–3955, 2009.

[3] Y. Chen, J. Jakeman, C. Gittelson, and D. Xiu. Local polynomial chaos expansion for linear differential equations with high dimensional random inputs. *SIAM J. Sci. Comput.*, 37(1):A79A102, 2015.

[4] H. Cho, D. Venturi, and G. E. Karniadakis. Karhunen-Loève expansion for multi-correlated stochastic processes. *Prob. Eng. Mech.*, 34:157–167, 2013.

[5] Q. Deng. An analysis for a nonoverlapping domain decomposition iterative procedure. *SIAM J. Sci. Comput.*, 18:1517–1525, 1997.

[6] H. Elman, D. G. Furnival, and C. E. Powell. $H(\mathrm{div})$ preconditioning for a mixed finite element formulation of the diffusion problem with random data. *Mathematics of Computation*, 79(270):733–760, 2010.

[7] H. Elman and Q. Liao. Reduced basis collocation methods for partial differential equations with random coefficients. *SIAM/ASA J. Uncertainty Quantification*, 1:192–217, 2013.

[8] O. G. Ernst, A. Mugler, H.-J. Starkloff, and E. Ullmann. On the convergence of generalized polynomial chaos expansions. *ESAIM: Math. Model. Numer. Anal.*, 46(2):317–339, 2012.

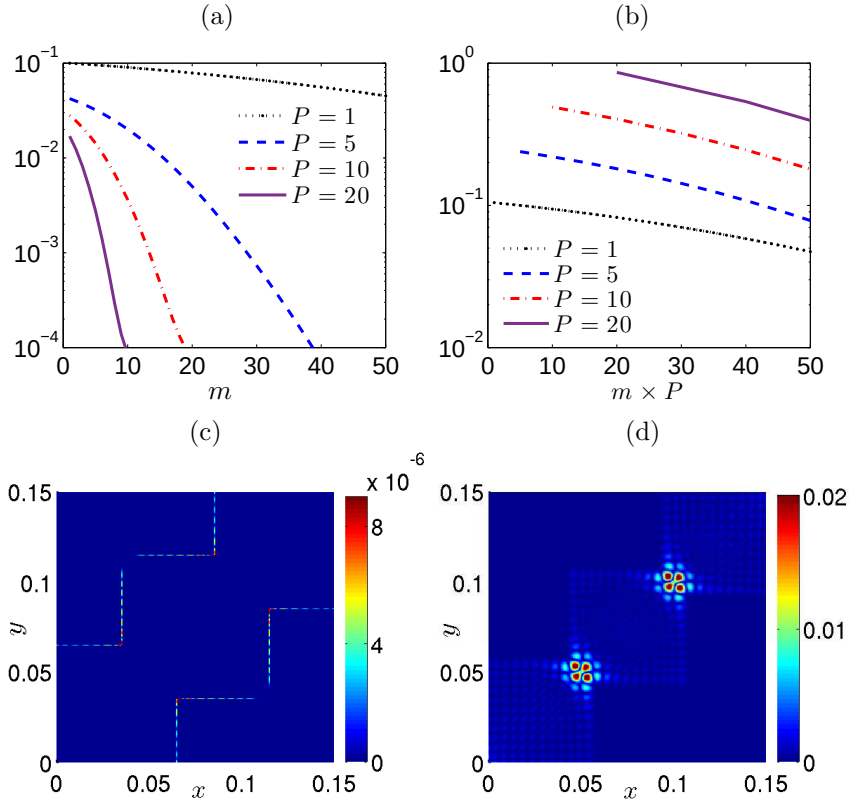

FIG. A.1. *Local K-L expansion: Relative L_2 errors in representing the covariance function for different number of subdomains P. In Fig. (a) we plot the error in each subdomain versus the number of local random variables m. In Fig. (b) we show the error in reconstructing the covariance in the whole domain $\mathcal{D}$ from the local covariances versus the total number of random variables $m \times P$. In (c) and (d), the absolute errors of the covariance related to ε_C and ε_i, respectively, are plotted for the case $P = 20$.*

[9] A. I. Fleishman. A method for simulating non-normal distributions. *Psychometrika*, 43:521–532, 1978.

[10] J. Foo and G. E. Karniadakis. The multi-element probabilistic collocation method (ME-PCM): Error analysis and applications. *J. Comput. Phys.*, 227:9572–9595, 2008.

[11] J. Foo and G. E. Karniadakis. Multi-element probabilistic collocation method in high dimensions. *J. Comput. Phys.*, 229:1536–1557, 2010.

[12] M. J. Gander, L. Halpern, and F. Nataf. Optimal Schwarz waveform relaxation for the one dimensional wave equation. *SIAM J. Numer. Anal.*, 41(5):1643–1681, 2003.

[13] M. J. Gander, F. Magoules, and F. Nataf. Optimized Schwarz methods without overlap for the Helmholtz equation. *SIAM J. Sci. Comput.*, 24(1):38–60, 2002.

[14] L. Gerardo-Giorda, F. Nobile, and C. Vergara. Analysis and optimization of Robin-Robin partitioned procedures in fluid-structure interaction problems. *SIAM J. Num. Anal.*, 48(6):2091–2116, 2010.

[15] A. Guadagnini, L. Guadagnini, D. M. Tartakovsky, and C. L. Winter. Random domain decomposition for flow in heterogeneous stratified aquifers. *Stoch. Environ. Res. Risk Assess*, 17(6):394407, 2003.

[16] M. D. Gunzburger and H. K. Lee. An optimization-based domain decomposition method for the navier-stokes equations. *SIAM J. Numer. Anal.*, 5:1455–1480, 2000.

[17] T. Hagstrom, R. P. Tewarson, and A. Jazcilevich. Numerical experiments on a domain decomposition algorithm for nonlinear elliptic boundary value problems. *Appl. Math. Lett.*, 1(3):299–302, 1988.

[18] S. Izvekov. Microscopic derivation of particle-based coarse-grained dynamics. *J. Chem. Phys.*, 138:134106(1–16), 2013.
[19] G. E. Karniadakis, A. Beskok, and N. Aluru, editors. *Microflows and nanoflows: fundamentals and simulation*. Springer, 2007.
[20] G. E. Karniadakis and S. Sherwin. *Spectral/hp element methods for computational fluid dynamics*. Oxford University Press, 2005.
[21] M. A. Katsoulakis, A. J. Majda, and A. Sopasakis. Intermittency, meatastability and coarse graining for coupled deterministic-stochastic lattice systems. *Nonlinearity*, 19:1021–1047, 2006.
[22] M. A. Katsoulakis, A. J. Majda, and D. G. Vlachos. Stochastic and mesoscopic models for tropical convection. *Proc. Natl. Acad. Sci. USA*, 100(3):782–787, 2003.
[23] B. Khouider, A. J. Majda, and M. A. Katsoulakis. Coarse-grained stochastic models for tropical convection and climate. *Proc. Natl. Acad. Sci. USA*, 100(21):11941–11946, 2003.
[24] S. Prudhomme L. Chamoin, J. T. Oden. A stochastic coupling method for atomic-to-continuum monte-carlo simulations. *Comput. Methods Appl. Mech. Engrg.*, 197:35303546, 2008.
[25] H. Lei, B. Caswell, and G. E. Karniadakis. Direct construction of mesoscopic models from microscopic simulations. *Phys. Rev. E*, 81(026704):1–10, 2010.
[26] G. Lin, A. M. Tartakovsky, and D.M. Tartakovsky. Uncertainty quantification via random domain decomposition and probabilistic collocation on sparse grids. *J. Comput. Phys.*, 299(19):69957012, 2010.
[27] J. Nash. Non-cooperative games. *Ann. Math.*, 54:286–295, 1951.
[28] F. Nobile, R. Tempone, and C. Webster. A sparse grid stochastic collocation method for partial differential equations with random input data. *SIAM J. Numer. Anal.*, 46(5):2309–2345, 2008.
[29] D. Olson, P. Bochev, M. Luskin, and A. V. Shapeev. Development of an optimization-based atomistic-to-continuum coupling method. In *Large-Scale Scientific Computing*, pages 33–44. Springer, 2014.
[30] D. Olson, P. Bochev, M. Luskin, and A. V. Shapeev. An optimization-based atomistic-to-continuum coupling method. *SIAM Journal on Numerical Analysis*, 52(4):2183–2204, 2014.
[31] D. Olson, A. V. Shapeev, P. Bochev, and M. Luskin. Analysis of an optimization-based atomistic-to-continuum coupling method for point defects. *arXiv preprint arXiv:1411.4027*, 2014.
[32] A. Quarteroni and A. Valli. *Domain decomposition methods for partial differential equations*. Oxford, 1999.
[33] S. S. Rao. Game theory approach for multiobjective structural optimization. *Computers & Structures*, 25(1):119–127, 1987.
[34] A. Sarkar, N. Benabbou, and R. Ghanem. Domain decomposition of stochastic PDEs: theoretical formulations. *Int. J. Numer. Meth. Engng.*, 77(5):689–701, 2009.
[35] B. Smith, P. Bjørstad, and W. Gropp. *Domain decomposition: parallel multilevel methods for elliptic partial differential equations*. Cambridge University Press, 1996.
[36] R. K. Sundaram. *A first course in optimization theory*. Cambridge Univ. Press, 2004.
[37] E. B. Tadmor and R. E. Miller. *Modeling materials: continuum, atomistic and multiscale techniques*. Cambridge University Press, 2011.
[38] D. M. Tartakovsky and S. Broyda. PDF equations for advective-reactive transport in heterogeneous porous media with uncertain properties. *Journal of Contaminant Hydrology*, 120-121:129140, 2011.
[39] S. Torquato. *Random Heterogeneous Materials: Microstructure and Macroscopic Properties*. Springer-Verlag (New York), 2002.
[40] A. Toselli and O. Widlund. *Domain Decomposition Methods - Algorithms and Theory*. Springer Series in Computational Mathematics, 2004.
[41] D. Venturi. On proper orthogonal decomposition of randomly perturbed fields with applications to flow past a cylinder and natural convection over a horizontal plate. *J. Fluid Mech.*, 559:215–254, 2006.
[42] D. Venturi. A fully symmetric nonlinear biorthogonal decomposition theory for random fields. *Physica D*, 240(4-5):415–425, 2011.
[43] D. Venturi and G. E. Karniadakis. Convolutionless Nakajima-Zwanzig equations for stochastic analysis in nonlinear dynamical systems. *Proc. R. Soc. A*, 470(2166):1–20, 2014.
[44] D. Venturi, D. M. Tartakovsky, A. M. Tartakovsky, and G. E. Karniadakis. Exact PDF equations and closure approximations for advective-reactive transport. *J. Comput. Phys.*, 243:323–343, 2013.
[45] D. Venturi, X. Wan, and G. E. Karniadakis. Stochastic bifurcation analysis of Rayleigh-Bénard

convection. *J. Fluid. Mech.*, 650:391–413, 2010.
[46] D. Venturi, X. Wan, R. Mikulevicious, B. L. Rozovsky, and G. E. Karniadakis. Wick-Malliavin approximation to nonlinear stochastic partial differential equations: analysis and simulations. *Proc. R. Soc. A*, 469(2158):1–20, 2013.
[47] H. von Stackelberg. *Market structure and equilibrium*. Springer, 2011.
[48] X. Wan and G. E. Karniadakis. Multi-element generalized polynomial chaos for arbitrary probability measures. *SIAM J. Sci. Comput.*, 28(3):901–928, 2006.
[49] C. L. Winter and D. M. Tartakovsky. Mean flow in composite porous media. *Geophys. Res. Lett.*, 27(12):17591762, 2000.
[50] D. Xiu and G. E. Karniadakis. The Wiener–Askey polynomial chaos for stochastic differential equations. *SIAM J. Sci. Comput.*, 24(2):619–644, 2002.
[51] D. Xiu and D.M. Tartakovsky. A two-scale nonperturbative approach to uncertainty analysis of diffusion in random composites. *Multiscale Model. Simul.*, 2(4):662–674, 2004.
[52] J. Xu. Iterative methods by space decomposition and subspace correction. *SIAM Review*, 34(4):581–613, 1992.
[53] J. Xu and J. Zou. Some nonoverlapping domain decomposition methods. *SIAM Review*, 40:857–914, 1998.
[54] Y. Yoshimoto, I. Kinefuchi, T. Mima, A. Fukushima, T. Tokumasu, and S. Takagi. Bottom-up construction of interaction models of non-Markovian dissipative particle dynamics. *Phys. Rev. E*, 88(043305):1–12, 2013.